

---

# Coarse-graining via reparametrization avoids force matching and back-mapping

---

**Nima Dehmamy**  
IBM Research  
Nima.Dehmamy@ibm.com

**Csaba Both**  
Northeastern University  
both.c@northeastern.edu

**Subhro Das**  
IBM Research  
subhro.das@ibm.com

**Tommi Jaakkola**  
MIT CSAIL  
tommi@csail.mit.edu

## Abstract

Energy minimization problems are highly non-convex problems at the heart of physical sciences. These problems often suffer from slow convergence due to sharply falling potentials, leading to small gradients. To make them tractable, we often resort to coarse-graining (CG), a type of lossy compression. We introduce a new way to perform CG using reparametrization, which does not require the costly steps of force-matching and back-mapping required in traditional CG. We focus on improving the slow dynamics by using CG to projecting onto slow modes. We also propose a way to find robust slow modes for many physical potentials. Our method also does not require data, which is expensive in molecular systems and a bottleneck for applying machine learning methods to such systems. We test our method on molecular dynamics for folding of small proteins. We observe that our method either reaches deeper (more optimal) energies or runs in shorter time than the baseline non-CG simulations.

In statistical physics we are interested in knowing in the most likely states the system will be in, given a set of exogenous factors (e.g. finding protein conformations at different temperatures, pH levels, etc) [12]. The negative log-likelihood function, or “free energy”, is based on physical laws, with more likely states having lower free energies. These systems generally have a large number of degrees of freedom (DOF) with complex interactions, making the free energy landscape high dimensional and highly non-convex. One way to make these problems tractable is to compress the DOF via coarse-graining (CG) [21, 18]. CG aims to reduce the degrees of freedom (DOF) in the system and replace them with clustered or collective modes. CG methods have proven very successful [19] in many fields such as molecular dynamics (MD) [7]. Yet, they also involve costly steps, such as back-mapping to fine-grained (FG) modes and force-matching [8].

In this paper we introduce a new approach to CG that allows us to find deeper energy levels more efficiently. Instead of replacing DOF with CG modes, we reparametrize the FG modes as functions of the CG modes. This approach allows us to both have access to FG modes at all times (avoiding back-mapping) and to compute forces without requiring force-matching. We choose our CG modes to be the “slow modes”, which are collective modes that evolve very slowly. Slow modes are the main cause of slow convergence of many problems, including MD. Additionally, slow modes may change during optimization, making it costly to keep track of and remedy them. In this work we show theoretically that in many physical systems, there exist robust slow modes, which change very little during optimization. We use these slow modes for our CG reparametrization. This allows us to first do the hard and slow part of the optimization without interference from fast modes. In the end, we allow all FG modes to relax, including the fast modes, to further optimize the solution. We show experimental results for MD simulations, where we find the reparametrized models achieve deeper energy levels or converge in shorter times, or both. In summary, our contributions are:

1. **CG via reparametrization:** a new method avoiding force-matching and back-mapping.
2. **Robust slow modes:** we devise a method for finding these modes in many systems.

3. **MD simulations:** we show the benefits of our method in protein MD simulations.
4. **Data-free:** our method modifies the optimization process and requires no training data.

## 1 Background

To find likely states in physical models we can minimize the free energy. Unlike optimization problems encountered in deep neural networks, these physics-based models are “shallow” by construction and usually do not have any input output data. The trainable “weights” are the physical DOF that need to be optimized, and the loss function is the free energy, which encodes all the nonlinear interactions of the weights. Usually, the interactions have multiple scales of strength. For instance, in MD covalent bonds are very strong, modeled as quadratic potentials  $\|r - r_0\|^2$ , while van der Waals forces between neutral atoms are extremely weak, falling sharply and modeled as Lennard-Jones (LJ) potentials  $c(r^{-12} - r^{-6})$ .

The hierarchy of forces makes the energy minimization quite challenging, including slow convergence of gradient-based methods. It leads to the system having fast and slow modes, with extremely large and small forces, respectively. The fast modes force us to choose small time steps for numerical stability, resulting in slow modes converging extremely slowly. To accelerate such free energy minimization problems we need to address the slow convergence of these slow modes. Two commonly taken approaches to address this issue are: 1) preconditioning (e.g. adaptive gradient or quasi-Newton method); 2) Coarse-graining (truncating the DOF to remove some fast modes). We focus on the second option here. Refer to sec. B for discussion on why adaptive gradient methods do not fully resolve the slow modes issue in physics problems.

### 1.1 Coarse-graining

CG involves a lossy compression which replaces the original DOF with new collective modes. We will be mostly considering what is called “bottom-up” CG (see [8] for a review). In MD, specifically, CG generally involves the following steps:

1. **Defining CG modes:** usually, a local clustering of multiple atoms into larger “beads”
2. **Force-matching:** finding the effective forces between CG modes resulting from FG forces.
3. **CG dynamics:** running MD for the CG modes with matched forces.
4. **Back-mapping:** from CG to the FG modes. Involves sampling, satisfying physical constraints, and minimizing the FG potentials.

CG generally removes the microscopic DOF responsible for the fast modes. CG can reduce simulation cost by both reducing the number of degrees of freedom, as well as by effectively removing some of the fast modes. However, the sampling and optimization in the back-mapping step can be quite expensive. As we show, our approach avoids the sampling and simplifies the fine-graining step.

**Choice of CG modes.** There exist various methods for choosing CG modes, depending on what information we wish to preserve. For example, in protein-folding, discretizing the conformation space into states and the transition probabilities between them yields a Markov model [6]. The spectrum of the Markov transition matrix captures the dynamics of the system. The eigenvalues correspond to the time scale (the rates of transitions between states), while the eigenvectors guide a clustering of states based on kinetic similarity [9, 22]. Other choices for CG modes include local clustering of atoms into beads, and using PCA on a matrix of multiple configurations to find co-moving parts [25]. In this work, we use the spectrum of a canonical Hessian to define the CG modes.

**Force-matching.** Force-matching requires us to find an effective potential such that forces between CG modes approximate the overall forces between their constituent FG modes. For a review of various classic force-matching algorithms, refer to [8]. Recently, machine learning methods have also been used to learn the force-matching potential [17, 11].

**Back-mapping.** The step to revert from CG modes to atomistic FG modes. Current methods build on geometric reconstruction [14] and refinement with MD [1, 20] or data-driven approaches [24, 23]. The main limitation of MD is speed, while the data-driven models are hard to generalize for complex large structures and require a large amount of data.

**Need for non-data-driven approaches.** Many ML approaches are data-driven and rely on availability of large amounts of high quality data. However, in problems such as material and molecular design data can be scarce or expensive to simulate. Importantly, the space of possible structures is so large that building datasets with good coverage is not feasible in many cases. Even for proteins, which are heavily researched, conformation data is scarce and protein-folding remained a difficult problem until recently. Our goal is to devise a methodology for improving energy minimization problems without the need for any training data.

## 2 Coarse-graining by reparametrization

Let  $X \in \mathcal{X} \simeq \mathbb{R}^{n \times d}$  be a set of DOF, e.g. particle positions, bond angles, etc. Let  $\mathcal{L} : \mathcal{X} \rightarrow \mathbb{R}$  be a loss function, which we will call the energy or potential. Our goal is either to simulate the dynamics of the system based on  $\mathcal{L}$ , or to find high likelihood configurations  $X^*$ , which are deep local minima of  $\mathcal{L}$ . Usually  $n$  is large and  $\mathcal{L}$  is a very steep non-convex function, making computations slow. Traditional CG involves mapping to a reduced space of CG variables,  $Z \sim \mathbb{R}^{k \times d}$  with  $k \ll n$ . But to run the dynamics using CG modes we need to figure out forces between CG modes, or “force-matching”, and how to go back to  $\mathcal{X}$ , or “back-mapping”.

**Force-matching.** The microscopic energy function is  $\mathcal{L} : \mathcal{X} \rightarrow \mathbb{R}$ . However, as CG replaces the DOF, we need to find an approximate potential  $\mathcal{L}_{CG} : \mathcal{Z} \rightarrow \mathbb{R}$  such that for  $X \in \mathcal{X}$  we have

$$\text{CG: } \phi : \mathcal{X} \rightarrow \mathcal{Z}, \quad \mathcal{L}_{CG}(\phi(X)) \approx \mathcal{L}(X). \quad (1)$$

The process of finding  $\mathcal{L}_{CG}$  is called force-matching. Traditional force-matching methods involve analytically solving and approximating  $\mathcal{L}_{CG}$  [8]. Recently, machine learning (ML) has been used to do force-matching for MD with good results [15, 11]. Next, the dynamics is run using  $\mathcal{L}_{CG}$  instead of  $\mathcal{L}$ .

**Back-mapping.** After the dynamics is run, we need to map back from  $\mathcal{Z}$  to  $\mathcal{X}$ . However, the map  $\rho : \mathcal{Z} \rightarrow \mathcal{X}$  is not unique, as generally many different  $X$  can be compressed to a given CG mode  $Z$ . Also, when going from  $Z$  to a possible  $X$ , some  $X$  may not be allowed (e.g. have overlapping atoms) or have large energies. Therefore, back-mapping usually involves sampling or optimization to find the allowed  $X$ . This can be challenging when there are many  $X$  mapping to the same  $Z$ . For instance, in protein dynamics most CG methods replace all atoms in each side chains with a single bead at their center of mass.

### 2.1 CG using reparametrization

Our idea to overcome the challenges of CG is to change the DOF  $X$  to a function of the CG modes, meaning we reparametrize  $X$  as

$$\text{Reparametrization: } X = \rho(Z), \quad \rho : \mathcal{Z} \rightarrow \mathcal{X} \quad (2)$$

which is the reverse of what traditional CG does. The advantages of this approach are:

1. **No back-mapping:** we have direct access to the fine-grained modes as  $X = \rho(Z)$ .
2. **No force-matching:** The energy for CG modes is  $\mathcal{L}_{CG}(Z) = \mathcal{L}(X) = \mathcal{L}(\rho(Z))$ .

One disadvantage of this approach is that we still use  $X$  to compute  $\mathcal{L}_{CG}(Z)$ . Nevertheless, if the CG leads to fewer optimization steps overall, or allows us to find deeper minima more efficiently, the benefits can outweigh the costs. Additionally, this cost could be reduced if  $\mathcal{L}_{CG}(Z)$  could be learned from  $\mathcal{L}(X)$ . We will not do so in this work, but discuss this as a future direction. Next we discuss the reparametrization function  $\rho$ .

**Choice of reparametrization.**  $\rho$  can be either an explicit and fixed function, or it can be a trainable neural network. The choice of  $\rho$  can depend on what quality or what property of  $X$  we want the CG modes to have. In our case, we are interested in energy minimization problems. So we want the choice of  $\rho$  to facilitate finding deeper energies or simplify the optimization problem. As mentioned above and elaborated in sec. B, a major bottleneck in energy minimization are the “slow modes”. As mentioned earlier, fast modes force us to choose smaller time steps. If we ignore fast modes in early stages of the optimization, we could traverse much larger time intervals. Therefore, we choose our

reparametrization  $\rho$  to be simply a linear projection onto slow modes

$$\text{Slow mode projection: } X = \rho(Z) = Z^T \Psi_{\text{Slow}} \equiv \sum_{i \in \text{Slow}} Z_i^T \psi_i \quad (3)$$

where  $\Psi = (\psi_i)_{i \in \text{Slow}}$  form a basis for **Slow**, the subspace spanned by slow modes, discussed next.

## 2.2 The Hessian backbone and robust slow modes

Before discussing the theoretical underpinning of our choice of slow modes, we will state how we find them in practice. As we show in sec. C, the slow modes are Hessian eigenvectors with eigenvalues close to zero. But since the Hessian  $H(X) = \nabla \nabla \mathcal{L}(X)$  depends on  $X$ , the slow modes can change during the dynamics. Nevertheless, we show that many physical energies, including in MD, have a special structure which allows us to find a set of robust slow modes. These slow modes should remain reliable for a long interval during optimization.

**Aggregating sampled Hessians.** To find a set of robust, approximate slow modes, we first compute the Hessian for a few perturbed configurations  $\text{Samples}(X) = \{X' = X + \delta X\}$ , where  $X$  is the current state and  $\delta X_i^\mu \sim \mathcal{N}(0, \sigma)$  is sampled from Gaussian ( $i$  is the particle index and  $\mu$  the spatial dimension). We want to extract a set of slow modes from the sampled Hessians  $H(X')$ . We then compute a backbone from these Hessians of the form

$$\text{Backbone: } \mathbf{H}_{ij} = \sum_{X' \in \text{Sample}(X)} \|H_{ij}(X')\|^2 \quad (4)$$

Here  $i, j \in \mathbb{Z}_n$  are the particle indices and the Frobenius norm  $\|H_{ij}\|^2 = \sum_{\mu, \nu} (H_{ij}^{\mu\nu})^2$  sums over the feature indices (note that  $X_i^\mu$  has a particle index  $i$  and a feature index  $\mu \in \{1, \dots, d\}$ ). Then, we extract the slow modes of the backbone, by doing a spectral expansion  $\mathbf{H} = \sum_i \lambda_i \psi_i \psi_i^T$  and picking  $\psi_i$  with  $|\lambda_i| < \varepsilon^2 \max_j |\lambda_j|$ , for some small  $\varepsilon < 1$ .

The intuition behind equation 4 is to identify the components in the sampled Hessians which have consistently high magnitudes. If we had taken a simple mean we could get very small values, because the components can fluctuate randomly. Also, if we had taken the variance instead of the norm, we would get zero for quadratic  $\mathcal{L}$ , where  $H$  is constant and has no variance. However, these intuitions do not show that there would be any connection between the modes of the backbone  $\mathbf{H}$  and the actual Hessians  $H(X')$ . Importantly, entries in  $H(X')$  have signs, which affects the spectrum, whereas all entries in  $\mathbf{H}$  are positive. So why should the spectra of  $H$  and  $\mathbf{H}$  be related? This is where the structure of  $\mathcal{L}$  comes into play. Indeed, we show in appendix C, for many physical  $\mathcal{L}$ , the slow modes of the backbone  $\mathbf{H}$  approximate the slow modes of sampled  $H(X')$  up to  $O(\varepsilon^2)$  errors (see appendix C.1 for proof).

## 3 Experiments

We apply our method to protein folding using classical MD forces.

**Settings:** We use gradient descent to minimize  $\mathcal{L}(X)$ . All experiments (both CG and baseline) use the Adam optimizer with a learning rate  $10^{-2}$  and early stopping with  $|\delta \mathcal{L}| = 10^{-6}$  tolerance and 5 steps patience. We run each experiment four times.

**Baseline:** we use direct GD on the MD energy as baseline.

**CG model:** We use four different choices for the fraction of the eigenvectors to use in CG equation 3:  $3 \times (\# \text{AminoAcids})$ , 30%, 50%, and 70%. We use a two stage process. First, we use CG as in equation 3  $X = \rho(Z) = Z^T \Psi_{\text{Slow}}$  and minimize  $\mathcal{L}_{CG}(Z) = \mathcal{L}(\rho(Z))$  over  $Z$ . After this stage converges to  $X_0 = \rho(Z_0)$ , we add  $\delta X$  to  $X_0$  and optimize the fine-grained  $\delta X$ , starting with  $\delta X = 0$ . In this FG step the loss reduces by a small, but noticeable, amount. For the CG step we choose a more relaxed stopping criteria  $|\delta \mathcal{L}_{CG}| = 10^{-5}$ , but use the same learning rate.

**Protein folding with classical MD** In protein folding our energy function consists of five potential energies for: bond length  $E_{bond}$ , bond angles  $E_{angle}$ , Van der Waals  $E_{vdW}$ , hydrophobic  $E_{hp}$  and hydrogen bonding  $E_H$  [2]. Note that we are ignoring the solvent (e.g. water) and writing using potentials, or force fields. To calculate the force field, we use distance,  $r$ , and angle-based,  $\Theta$ , potentials. For each amino acid, we use the rdkit [13] package to acquire bond length,  $r_0$ , and bond angle,  $\theta_0$  (every triplet of atoms defining the bond), information that we use to define

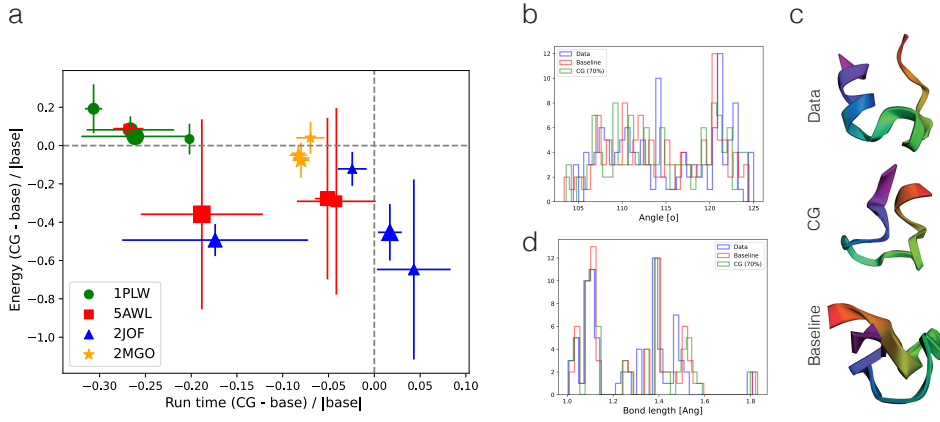


Figure 1: (a) time vs. energy of CG runs relative to the baseline. The symbol sizes encode different numbers of eigenvectors in CG. The different colors and symbols correspond to different proteins: 5AWL, 1PLW, 2JOF, and 2MGO. (b) The angle and (d) bond length distribution of 1PLW protein acquired from the data and calculated by using the baseline and CG (70%) methods. (c) The native structure (data) of the 2JOF protein, and the layouts obtained from the baseline and CG method.

quadratic energies  $E_{bond}$  and  $E_{angle}$ . We use Lennard-Jones (LJ) potentials,  $V_{p,q}(r) = r^{-p} - r^{-q}$ , to approximate  $E_{vdW}$  between all pairs of atoms,  $E_H$  between atoms prone to form a hydrogen bond (certain  $H$  and  $O$ , in our case),  $E_{hp}$  between atoms in hydrophobic residues, yielding

$$\begin{aligned}
 \mathcal{L}(X) &= E_{bond} + E_{angle} + E_{vdW} + E_H + E_{hp} \\
 &= k_{bond}(r - r_0)^2 + k_{angle}(\theta - \theta_0)^2 \\
 &\quad + \epsilon_{vdW} V_{12,6} \left( \frac{r}{\sigma_{vdW}} \right) + \epsilon_H V_{6,4} \left( \frac{r}{\sigma_H} \right) + \epsilon_{hp} V_{6,4} \left( \frac{r}{\sigma_{hp}} \right)
 \end{aligned} \tag{5}$$

Here the coupling matrix  $[\sigma_{vdW}]_{ij} = a_i + a_j$  where  $a_i$  is the vdW radius of atom  $i$ . For atoms which form H-bonds,  $[\sigma_H]_{ij} = (b_i \cdot b_j)1.5\text{\AA}$  (hydrogen bonding radius) with  $b_i = 1$  if  $i$  forms an H-bond, and  $b_i = 0$  otherwise.  $[\sigma_{hp}]_{ij} = c_i + c_j$  where  $c_i = 2\text{\AA}$  if atom  $i$  is in a hydrophobic residue and  $c_i = 0$  otherwise. Figure 2 shows an example of these coupling matrices for the Enkephalin (1PLW) protein. We implemented a framework to build peptide chains using the 20 universal amino acids where we connect them by peptide bonds. To evaluate the effect of our CG model, we run experiments on four small proteins: Chignolin (5AWL), Trp-Cage (2JOF), Cyclotide (2MGO) and Enkephalin (1PLW).

**Results.** We run each experiment four times. Denoting the final energy and run time of the CG model by  $E_{CG}$  and  $t_{CG}$ , ad baseline by  $E_0$  and  $t_0$ , we compute the normalized differences  $\delta\hat{E} = (E_{CG} - E_0)/E_0$  and  $\delta\hat{t} = (t_{CG} - t_0)/t_0$ . The normalization allows us to plot results from different proteins together. Figure 1a shows the mean of  $\delta\hat{E}$  vs  $\delta\hat{t}$  over the 4 runs for each CG setting. The cross shows the spread (1 STD) over the four runs for energy and time. Overall we find that all CG models outperform the baseline either in terms of run time or energy, or both. We note that our choices for  $\epsilon_H$ ,  $\epsilon_{vdW}$ ,  $\epsilon_{hp}$  and  $k_{bond}$ ,  $k_{angle}$ , can be a source of error. Additionally, we “softened” the LJ potential to  $V_{p,q} = 1/(r^p + \zeta) - 1/(r^q + \zeta)$  with  $\zeta = 0.65$ , which is large and significantly reduces the penalty for overlapping atoms and may reduce accuracy.

## 4 Discussion

We Showed preliminary evidence that CG through reparametrization can yield some improvements over non-CG baseline in protein folding, both in terms of run time as well as energy. This method has the advantage that it does not require force-matching or back-mapping. However, more experiments are needed to compare it against traditional CG methods. In fact, using ML to learn force-matching might provide further advantage by removing the need to evaluate  $\mathcal{L}_{CG}(Z) = \mathcal{L}(X)$  via the fine-grained modes  $X$ . Also, while our canonical slow modes are derived for physical Hessians, the reparametrization approach to CG is general and could be applied to other ML problems.

## References

- [1] Aleksandra E Badaczewska-Dawid, Andrzej Kolinski, and Sebastian Kmiecik. Computational reconstruction of atomistic protein structures from coarse-grained models. *Computational and structural biotechnology journal*, 18:162–176, 2020.
- [2] G Ceci, A Mucherino, M D’Apuzzo, Daniela Di Serafino, S Costantini, A Facchiano, and G Colonna. Computational methods for protein fold prediction: an ab-initio topological approach. *Data Mining in Biomedicine*, pp. 391–429, 2007.
- [3] John Duchi, Elad Hazan, and Yoram Singer. Adaptive subgradient methods for online learning and stochastic optimization. *Journal of machine learning research*, 12(7), 2011.
- [4] Roger Fletcher. *Practical methods of optimization*. John Wiley & Sons, 2013.
- [5] Vineet Gupta, Tomer Koren, and Yoram Singer. Shampoo: Preconditioned stochastic tensor optimization. In *International Conference on Machine Learning*, pp. 1842–1850. PMLR, 2018.
- [6] Nina Singhal Hinrichs and Vijay S Pande. Calculation of the distribution of eigenvalues and eigenvectors in markovian state models for molecular dynamics. *The Journal of chemical physics*, 126(24):244101, 2007.
- [7] Scott A Hollingsworth and Ron O Dror. Molecular dynamics simulation for all. *Neuron*, 99(6): 1129–1143, 2018.
- [8] Jaehyeok Jin, Alexander J Pak, Aleksander EP Durumeric, Timothy D Loose, and Gregory A Voth. Bottom-up coarse-graining: Principles and perspectives. *Journal of Chemical Theory and Computation*, 18(10):5759–5791, 2022.
- [9] Mary E Karpen, Douglas J Tobias, and Charles L Brooks III. Statistical clustering techniques for the analysis of long molecular dynamics trajectories: analysis of 2.2-ns trajectories of ypgdv. *Biochemistry*, 32(2):412–420, 1993.
- [10] Diederik P Kingma and Jimmy Ba. Adam: A method for stochastic optimization. *arXiv preprint arXiv:1412.6980*, 2014.
- [11] Andreas Krämer, Aleksander P Durumeric, Nicholas E Charron, Yaoyi Chen, Cecilia Clementi, and Frank Noé. Statistically optimal force aggregation for coarse-graining molecular dynamics. *arXiv preprint arXiv:2302.07071*, 2023.
- [12] Lev Davidovich Landau and Evgenii Mikhailovich Lifshitz. *Statistical Physics: Volume 5*, volume 5. Pergamon, 1980.
- [13] Greg Landrum, Paolo Tosco, Brian Kelley, sriniker, gedeck, NadineSchneider, Riccardo Vianello, Ric, Andrew Dalke, Brian Cole, AlexanderSavelyev, Matt Swain, Samo Turk, Dan N, Alain Vaucher, Eisuke Kawashima, Maciej Wójcikowski, Daniel Probst, guillaume godin, David Cosgrove, Axel Pahl, JP, Francois Berenger, strets123, JLVarjo, Noel O’Boyle, Patrick Fuller, Jan Holst Jensen, Gianluca Sforna, and DoliathGavid. rdkit/rdkit: 2020\_03\_1 (q1 2020) release, March 2020. URL <https://doi.org/10.5281/zenodo.3732262>.
- [14] Leandro E Lombardi, Marcelo A Martí, and Luciana Capece. Cg2aa: backmapping protein coarse-grained structures. *Bioinformatics*, 32(8):1235–1237, 2016.
- [15] Maciej Majewski, Adrià Pérez, Philipp Thölke, Stefan Doerr, Nicholas E Charron, Toni Giorgino, Brooke E Husic, Cecilia Clementi, Frank Noé, and Gianni De Fabritiis. Machine learning coarse-grained potentials of protein thermodynamics. *Nature Communications*, 14(1):5739, 2023.
- [16] James Martens and Roger Grosse. Optimizing neural networks with kronecker-factored approximate curvature. In *International conference on machine learning*, pp. 2408–2417. PMLR, 2015.
- [17] Julien Maupetit, P Tuffery, and Philippe Derreumaux. A coarse-grained protein force field for folding and structure prediction. *Proteins: Structure, Function, and Bioinformatics*, 69(2): 394–408, 2007.

- [18] William George Noid. Perspective: Coarse-grained models for biomolecular systems. *The Journal of chemical physics*, 139(9), 2013.
- [19] Alexander J Pak and Gregory A Voth. Advances in coarse-grained modeling of macromolecular complexes. *Current opinion in structural biology*, 52:119–126, 2018.
- [20] Jorge Roel-Touris and Alexandre MJJ Bonvin. Coarse-grained (hybrid) integrative modeling of biomolecular interactions. *Computational and structural biotechnology journal*, 18:1182–1190, 2020.
- [21] Marissa G Saunders and Gregory A Voth. Coarse-graining methods for computational biology. *Annual review of biophysics*, 42:73–93, 2013.
- [22] William C Swope, Jed W Pitner, and Frank Suits. Describing protein folding kinetics by molecular dynamics simulations. 1. theory. *The Journal of Physical Chemistry B*, 108(21): 6571–6581, 2004.
- [23] Wujie Wang, Minkai Xu, Chen Cai, Benjamin Kurt Miller, Tess Smidt, Yusu Wang, Jian Tang, and Rafael Gómez-Bombarelli. Generative coarse-graining of molecular conformations. *arXiv preprint arXiv:2201.12176*, 2022.
- [24] Soojung Yang and Rafael Gómez-Bombarelli. Chemically transferable generative backmapping of coarse-grained proteins. *arXiv preprint arXiv:2303.01569*, 2023.
- [25] Zhiyong Zhang, Lanyuan Lu, Will G Noid, Vinod Krishna, Jim Pfaendtner, and Gregory A Voth. A systematic methodology for defining coarse-grained sites in large biomolecules. *Biophysical journal*, 95(11):5073–5083, 2008.

## A Additional Figures

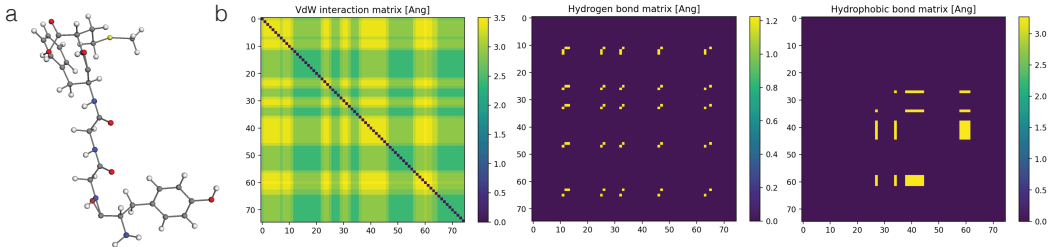


Figure 2: Enkephalin (1PLW). a) The peptide chain is built by stacking amino acids on each other using the peptide bond length from the literature, 1.32. b) Van der Waals, hydrogen bond, and hydrophobic interaction matrix, that we use in the energy optimization.

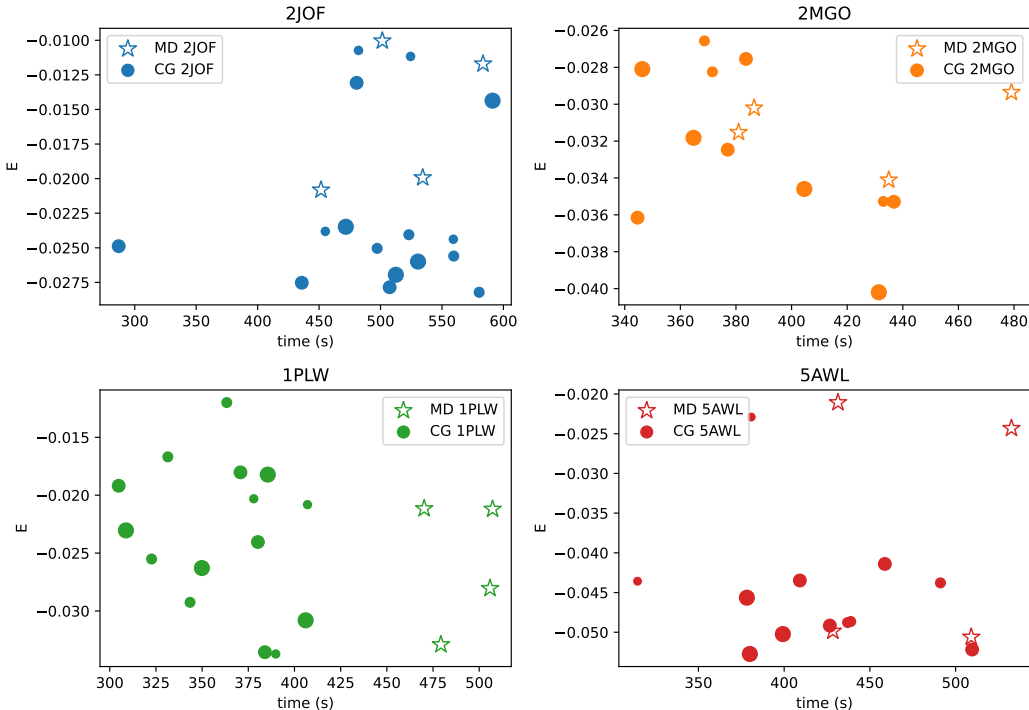


Figure 3: Comparison of performance of CG Hessian versus baseline MD. Point sizes correspond to the number of CG modes used.

## B Energy minimization

Let  $X \in \mathcal{X} \simeq \mathbb{R}^{n \times d}$  be a set of degrees of freedom (e.g. particle positions, bond angles, etc.) and let  $\mathcal{L} : \mathcal{X} \rightarrow \mathbb{R}$  be the energy (loss) function. We are interested in finding configurations  $X^*$  which are local minima of  $\mathcal{L}$ . We can find such  $X^*$  using a gradient descent (GD), or its continuous variant, gradient flow (GF)

$$\frac{dX}{dt} = -\varepsilon \nabla \mathcal{L}(X) \tag{6}$$

where  $\varepsilon$  is the matrix of learning rates (LR). In simple GD where  $\varepsilon = cI$  is a single constant times identity, GD evolves at different rates in different directions, with some being much slower than others. At a given  $X$ , these “slow modes” are the eigenvectors of the Hessian  $H(X) = \nabla \nabla \mathcal{L}(X)$  with eigenvalues closest to zero, as we review below. We will first define fast and slow modes in the simple quadratic case and then generalize them to non-convex cases in the next section.

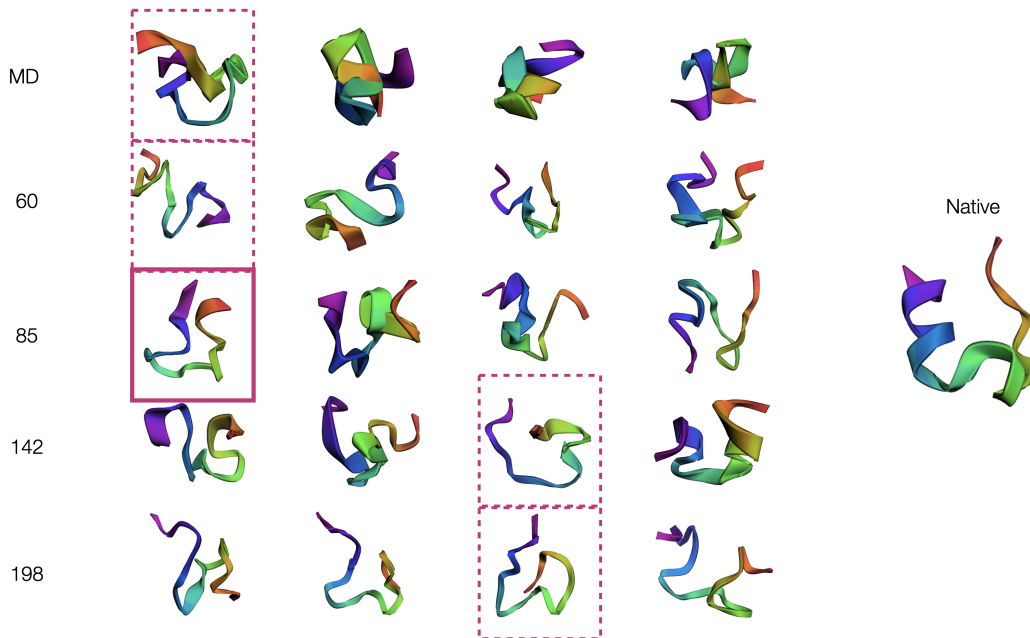


Figure 4: The folded structures of the 2JOF protein by using the CG and baseline method. The numbers in front of the rows are the numbers of eigenvectors used in the CG reparametrization. Dashed frames show the minimum energy embedding in each case, while the thick line frame highlights the absolute minimum layout.

**Fast and slow modes for quadratic Loss.** Consider the case where  $\mathcal{L}(X) = \frac{1}{2}\text{Tr}[X^T \mathbf{H} X]$ . Here  $\mathbf{H}$  is a Hermitian matrix and the Hessian of  $\mathcal{L}$ , with a spectral expansion given by  $\mathbf{H} = \sum_i \lambda_i \psi_i \psi_i^T$ ,  $\lambda_i \in \mathbb{R}$  and  $\psi_i \in \mathbb{R}^n$ . In this basis we have  $X(t) = \sum_i c_i(t) \psi_i$  with  $c_i : \mathbb{R} \rightarrow \mathbb{R}^d$ . Projecting equation 6 onto one of the eigenmodes we get

$$\frac{dc_i}{dt} = \psi_i^T \frac{dX}{dt} = -\varepsilon \lambda_i \psi_i^T X = -\varepsilon \lambda_i c_i \quad (7)$$

where we assumed  $d\psi_i/dt = 0$ . From equation 7 we see that the decay/growth rate along mode  $\psi_i$  is  $|\varepsilon \lambda_i|$ . Hence, modes with  $\lambda_i$  close to zero are the “slow modes”, evolving very slowly, and large  $|\lambda_i|$  defines the “fast modes”. Since  $c_i(t) = c_i(0) \exp[-t/\tau_i]$  with time scale  $\tau_i = 1/(\varepsilon \lambda_i)$ , the fast modes evolve exponentially faster than slow modes. This disparity in the rates results in slow convergence, because the fast modes force us to choose smaller  $\varepsilon$  to avoid numerical instabilities. Two potential ways to fix the issue with disparity in time scales are: 1) make rates isotropic (second-order methods and adaptive gradients); 2) mode truncation or compression (CG). We will briefly review the former here.

**Adaptive gradient and second-order methods.** Newton’s method uses  $\varepsilon = \eta H(X)^{-1}$  which makes GD isotropic along all modes, but it is expensive ( $O((3n)^3)$  in our case). Quasi-Newton methods, e.g. BFGS [4], approximate  $H^{-1}$  iteratively, but are generally also slow. Another, more efficient approach is adaptive gradient methods, such as AdaGrad [3] and Adam [10] which approximate  $H$  by  $\sqrt{g_t g_t^T + \eta}$  where  $g_t = \sum_{i=1}^k \gamma^i \nabla \mathcal{L}(X(t-i))$  is some discounted average over past gradients and  $\eta$  a small constant. For efficiency, in practice we only use the diagonal part of this matrix to approximate  $H^{-1}$ . As we will see in experiments, this approximation, while being far superior to GD with constant LR, is still very slow for MD tasks.

Most second-order methods are designed to work for generic problem and don’t make strong assumptions about the spectrum of the Hessian. Recent second-order methods such as K-FAC [16] and Shampoo [5] work with block diagonal approximations of the Hessian (or the Fisher information matrix), which usually emerges in deep learning models due to model architecture. Instead, we will exploit the spectral properties of the Hessian in physics problems. Fast and slow modes generally

arise in physics due to vastly different strengths in forces (e.g. weak van der Waals vs strong chemical bonds).

### B.1 Generalized fast and slow modes

The notion of fast and slow modes is helpful for the analysis of any time slice of the dynamics during which the Hessian is not changing dramatically. Consider a configuration  $X(t)$  and let  $\delta t$  be a small time interval. We are looking for modes which are almost stationary over  $\delta t$ . To identify these modes, we can for instance find perturbations  $\delta X$  which would have almost zero dynamics. concretely we find the dynamics of  $X + \delta X$  as

$$\frac{d}{dt}(X + \delta X) = -\varepsilon \nabla \mathcal{L}(X + \delta X) \approx -\varepsilon \nabla \mathcal{L}(X) - \varepsilon H \delta X + O(\delta X)^2 \quad (8)$$

meaning, a small  $\delta X$  adds  $\varepsilon H \delta X$  to the dynamics. Thus if  $\delta X$  is a zero mode of the Hessian,  $H \delta X = 0$ , it won't change the dynamics of  $X$ . To define slow modes, we can slightly relax this and look for normalized modes  $\psi = \delta X / \|\delta X\|$  whose associated time scale is much longer than a desired time scale  $\delta t$

$$\tau = |\varepsilon \psi^T H \psi| = |\varepsilon \lambda| \gg \delta t \quad (9)$$

which just means that we need to find the approximate zero modes of the Hessian  $H(X)$ .

**CG by projecting to the slow manifold.** Because the dynamics of the modes above is very slow over  $\delta t$ , we can safely increase the time scale and run their dynamics over much longer periods  $\Delta t \gg \delta t$ . The essence of our algorithm is to ignore fast modes and project and evolve the system on the ‘‘slow manifold’’ spanned by the slow modes of the Hessian. However, the main challenge is how to deal with the fact that the Hessian is not constant and depends on the configuration  $X$ . We address this point next. We show that for a large class of physical potentials one can find a reliable set of approximate slow modes.

## C Properties of Physical Hessians

**Invariant potentials.** In systems of interacting particles in physics, most of the leading interactions are pairwise and involve relative features,  $\mathbf{r}_{ij} \equiv X_i - X_j$  (distance vector, relative angle, etc). Moreover, they are often invariant under certain global symmetries, such as Euclidean symmetries (translation and rotation) or Lorentz symmetry (relativistic particles). These symmetries keep some 2-norm of vectors,  $v^2 = \|v\|_\eta \equiv v^T \eta v$  invariant. Here  $\eta$  may be the Euclidean metric  $\eta = \text{diag}(1, 1, 1)$  or the Minkowski metric  $\eta = \text{diag}(-1, 1, 1, 1)$  for relativistic problems, etc. For example, the Euclidean norm  $v^T v$  in  $d$  dimensions is invariant under rotations  $v \rightarrow gv$ , where  $g \in SO(d)$ , and the Minkowski norm is invariant under the Lorentz group  $SO(1, d-1)$ .

Let  $r$  denote the matrix of distances with  $r_{ij} = \|\mathbf{r}_{ij}\|_\eta$ . Any function of  $r_{ij}$  is invariant under symmetries that keep  $\|\cdot\|_\eta$  invariant. A general invariant energy function can combine  $r_{ij}$  for different  $i, j$  in arbitrary ways. Usually in physical systems each pair contributes an additive term in to the total energy. Assuming additivity, the energy has a form

$$\mathcal{L}(X) = \sum_{ij} f_{ij}(r_{ij}) \quad (10)$$

where  $f_{ij}(z) = f_{ji}(z)$  (symmetric under  $i \leftrightarrow j$ ). For example, when particle  $i$  has electric charge  $q_i$ , the Coulomb potential between  $i, j$  can be written as in equation 10 using  $f_{ij}(z) = kq_i q_j / z$ . Similarly, weak van der Waals (vdW) forces in molecular systems, which are modeled as Lennard-Jones potential, are also of the form in equation 10 with

$$\text{van der Waals: } f_{ij}(r_{ij}) = V_{p,q} \left( \frac{r_{ij}}{\sigma_{ij}} \right), \quad V_{p,q}(r) = \frac{1}{r^p} - \frac{1}{r^q}. \quad (11)$$

Here  $\sigma_{ij} = a_i + a_j$ , where  $a_i$  is the vdW radius of particle  $i$ , and vdW uses  $p = 12, q = 6$ . Next, we show that the Hessian of equation 10 has an important property which aids in finding its slow modes.

### C.0.1 Hessian of invariant potentials

The Hessian of potentials of the form equation 10 has the special property that it is the graph Laplacian of a weighted graph which depends on  $X$ , as we show now (see appendix D for details). This will play a crucial role in our argument about canonical slow modes.

**Hessian as a graph Laplacian.** Let  $\partial_i \equiv \partial/\partial X_i$  and let  $\hat{r} = \eta \mathbf{r}/r$  be the dual unit vector of  $\mathbf{r}$ . First, observe that  $\partial_i r_{jk} = \hat{r}_{jk}(\delta_{ij} - \delta_{ik})$  where  $\hat{r}_{jk}$  is the unit vector of  $\mathbf{r}_{jk}$  and  $\delta_{ij}$  is the Kronecker delta (1 if  $i = j$ , 0 otherwise). Let  $\text{Hes}[g]$  denote the Hessian of a function  $g$ . We find that (app. D)

$$\text{Hes}[\mathcal{L}](X)_{ij} = \partial_i \partial_j \mathcal{L}(X) = \sum_k (\delta_{ij} - \delta_{jk}) \mathbf{H}_{ik}(X) \quad (12)$$

where  $\mathbf{H}_{ik}(X) = \text{Hes}[f_{ik}](r_{ik})$  and given by

$$\mathbf{H}_{ik}(X) = \left[ \left( f''_{ik}(v) - \frac{f'_{ik}(v)}{v} \right) \hat{v} \otimes \hat{v} + \frac{f'_{ik}(v)}{v} \eta \right]_{\mathbf{v}=\mathbf{r}_{ik}} \quad (13)$$

Note that  $\mathbf{H}$  has four indices, with components  $\mathbf{H}_{ij}^{\mu\nu}$ , having two particle indices  $i, j$  and two spatial indices  $\mu, \nu$ . Recall the Laplacian of an undirected graph with adjacency matrix  $A$  is defined as  $L = \text{Lap}(A) = D - A$ , where  $D$  is the degree matrix with elements  $D_{ij} = \delta_{ij} \sum_k A_{ik}$ . The components of Laplacian can also be written as  $L_{ij} = \sum_k A_{ik}(\delta_{ij} - \delta_{jk})$ . Thus, we see that the Hessian of  $\mathcal{L}$  is indeed the Laplacian of  $\mathbf{H}$

$$\text{Hes}[\mathcal{L}](X)_{ij} = \sum_k (\delta_{ij} - \delta_{jk}) \mathbf{H}_{ik} = \text{Lap}(\mathbf{H})_{ij} \quad (14)$$

where for every pair of spatial indices the Hessian is a Laplacian over particle indices. The Hessian being Laplacian has an important effect on its null eigenvectors. To show this we make use of the incidence matrix.

### C.1 Canonical backbone for the Hessian

As the Hessian depends on  $X$ , it is not clear whether slow modes found at a given  $X$  would be applicable to other  $X$ . We need some guarantee that a set of modes exist which are approximately slow modes for the Hessian at a range of different  $X$ . We could use multiple perturbed configurations  $X + \delta X$  with random  $\delta X \sim \mathcal{N}(0, T)$  to get an ensemble of Hessians  $\mathcal{H} = \{H(X + \delta X)\}$  and find the overlap of the slow modes of the Hessians in  $\mathcal{H}$ . However, this is expensive, roughly  $O(mkn^2)$  for  $m = |\mathcal{H}|$  and  $k$  slow modes. We cannot recompute the Hessian slow modes often. We also want a method which is more efficient than quasi-Newton methods such as BFGS. Our solution is to find a backbone for the sampled Hessians whose slow modes are guaranteed to be approximate slow modes of the actual Hessians. The key observation is that the Hessian in equation 14 is a Laplacian of a weighted graph. We show that the slow modes of weighted Laplacians overlap significantly with their unweighted counterparts.

**Definition C.1** (weighted graph). Let  $\hat{\mathcal{G}} = (\mathcal{V}, \mathcal{E})$  be a graph with vertices  $\mathcal{V} = \mathbb{Z}_n$ , edges  $\mathcal{E} \subseteq \mathcal{V} \times \mathcal{V}$ . Let  $\hat{A} \in \mathbb{R}^{n \times n}$  denote the adjacency matrix  $\hat{A}_{ij} = 1$  if  $(i, j) \in \mathcal{E}$  and 0 otherwise. We denote a weighted graph as  $\mathcal{G} = (\mathcal{V}, \mathcal{E}, \mathcal{W})$  where  $\mathcal{W} : \mathcal{E} \rightarrow \mathbb{R}$  are the weights of the edges. Let  $A$  denote the adjacency matrix of  $\mathcal{G}$ , where  $A_{ij} = \mathcal{W}(i, j)$  or zero if  $(i, j) \notin \mathcal{E}$ . The Laplacian  $L = \text{Lap}(A)$  of an undirected weighted graph is defined analogous to the unweighted graph as  $L = D - A$  with degree matrix elements  $D_{ij} = \delta_{ik} \sum_k A_{ik}$ .

**Definition C.2** (Slow manifold). Let  $L$  be a graph Laplacian (undirected, weighted or unweighted), with spectral expansion  $L = \sum_{i=1}^n \lambda_i \psi_i \psi_i^T$ . Let  $\varepsilon \ll 1$  and  $\lambda_{\max} = \max\{\lambda_i\}$  be the largest eigenvalue of  $L$ . We define the slow manifold as

$$\mathbf{Slow}_\varepsilon[L] = \text{Span}\{\psi_i \mid |\lambda_i| < \varepsilon^2 \lambda_{\max}\} \quad (15)$$

**Theorem C.1** (Slow modes of weighted Laplacians). Let  $A$  be the adjacency matrix of a weighted graph and  $\hat{A}$  be its unweighted counterpart. Let  $L = \text{Lap}(A)$  and  $\hat{L} = \text{Lap}(\hat{A})$ . Then  $\mathbf{Slow}_\varepsilon[L]$  overlaps with  $\mathbf{Slow}_\varepsilon[\hat{L}]$  up to  $O(\varepsilon^2)$  corrections from the rest of the modes.

To prove this we will make use of the incidence matrix representation of the Laplacian.

**Definition C.3** (Incidence matrix). *Given a weighted graph  $\mathcal{G} = (\mathcal{V}, \mathcal{E}, \mathcal{W})$ , define its incidence matrix as  $C : \mathcal{V} \times \mathcal{E} \rightarrow \{\pm 1\}$ , where for any edge  $e = (i \rightarrow j) \in \mathcal{E}$ ,  $C_{i,e} = -1$  and  $C_{j,e} = 1$ , and zero for other components.*

**Lemma C.2** (Laplacian in terms of the incidence matrix). *Let  $w = \text{vec}(\mathcal{W}(\mathcal{E}))$  be the vector of all weights indexed in the same order as the columns of  $C$ , with  $w_e = A_{ij}$ , for  $e = (i, j)$  and let  $W$  be a diagonal matrix with  $w$  on its diagonal. Then, the Laplacian  $L = \text{Lap}(A)$  can be written as  $L = \frac{1}{2}CWC^T$  (proof in app. D.1).*

Because  $\mathcal{G}$  and  $\hat{\mathcal{G}}$  share the same vertices and edges, their incidence matrix  $C$  is the same. From Lemma C.2,  $L = \frac{1}{2}CWC^T$  and  $\hat{L} = \frac{1}{2}CC^T$  as  $\hat{\mathcal{G}}$  is unweighted. Using SVD,  $C = USV^T$  and defining  $R = US/\sqrt{2}$  and  $Q = V^T WV$ , we have

$$\hat{L} = RR^T \quad L = RQR^T. \quad (16)$$

Note that for a random configuration  $X$  the edge weights  $W$  will be random, as they arising from derivatives of  $f_{ij}(r_{ij})$  in equation 13 (unless  $f_{ij}$  is quadratic which makes  $W$  constant). Therefore, we will assume  $Q$  has a uniform Gaussian distribution. Assuming  $W$  is also Gaussian, the spectrum of such a  $Q = V^T WV$  is somewhere between the distribution of  $W$  (for sparse graphs with  $|\mathcal{E}| \sim O(|\mathcal{V}|)$ ) and a Wigner Semi-circle (for dense graphs with  $|\mathcal{E}| \sim O(|\mathcal{V}|^2)$ ). See appendix D.2 for more discussion. We also assume  $Q$  has no particular block structure and that the spectrum of any diagonal block of  $Q$  should also follows a distribution similar to all of  $Q$ .

**Slow subspace.** We now sketch the proof for Theorem C.1. For details, refer to appendix D.4. From the SVD,  $C = USV^T$ , the slow subspace is

$$\mathbf{Slow}_\varepsilon[\hat{L}] = \{i | S_{ii} < \varepsilon \max[S]\} \quad (17)$$

Normalize  $\hat{S} = S/\max[S]$  and make them all positive (e.g. absorb their sign into  $U$ ). For some  $\varepsilon < 1$  sort the SV such that  $\hat{S} = \text{diag}(S_\varepsilon, S_1)$  where the diagonal matrices  $S_\varepsilon < \varepsilon$  and  $S_1 \geq \varepsilon$ . Now, the problem of finding  $\mathbf{Slow}_\varepsilon[L]$  becomes finding eigenvectors of the matrix  $\hat{M} = \hat{S}Q\hat{S}^T$  with eigenvalues  $O(\varepsilon^2)$ . Using  $S_\varepsilon \sim O(\varepsilon)$  and  $S_1 \sim O(1)$ , we can pull factors of  $\varepsilon$  out from  $\hat{M}$  and write it as

$$\hat{M} = M_0 + \hat{\varepsilon}\delta M, \quad M_0 = \begin{pmatrix} \hat{\varepsilon}^2 \hat{A} & 0 \\ 0 & C \end{pmatrix}, \quad \delta M = \begin{pmatrix} 0 & \hat{B} \\ \hat{B}^T & 0 \end{pmatrix}. \quad (18)$$

where  $\hat{\varepsilon}^2 \equiv \varepsilon^2 \sqrt{n_A/n_C}$  is rescaled so that the random matrices  $\hat{A} \in \mathbb{R}^{n_A \times n_A}$  and  $C \in \mathbb{R}^{n_C \times n_C}$  have a similar range of eigenvalues. Next, using a perturbative ansatz for eigenvectors  $\psi' = \psi + \hat{\varepsilon}\delta\psi$  and eigenvalues  $\lambda' = \lambda + \hat{\varepsilon}\delta\lambda$ , we solve  $\hat{M}\psi' = \lambda'\psi'$  up to  $O(\hat{\varepsilon}^2)$  corrections.

To find slow modes for  $L$  we start from  $\psi \in \mathbf{Slow}_\varepsilon[\hat{L}]$ . Specifically, we start with an eigenvector  $\psi_A$  of  $\hat{A}$  and concatenate it with zeros to get  $\psi = (\psi_A, 0)$ . We have  $M_0\psi = \lambda\psi$  with  $\lambda = \hat{\varepsilon}^2\lambda_A$ . Using first-order perturbation theory, we find the corrections  $\delta\lambda$  to the eigenvalues and eigenvectors to be

$$\delta\lambda = \psi^T \delta M \psi = 0, \quad \delta\psi = -(M_0 - \lambda)^{-1} \delta M \psi = \begin{pmatrix} 0 \\ (C - \lambda)^{-1} \hat{B}^T \psi_A \end{pmatrix}. \quad (19)$$

Putting all together we find the slow eigenvector  $\psi' = \psi + \hat{\varepsilon}\delta\psi$  up to order  $O(\varepsilon^2)$  to be

$$\mathbf{Slow}_\varepsilon[L] \ni \psi' = \begin{pmatrix} \psi_A \\ \hat{\varepsilon}(C - \hat{\varepsilon}^2\lambda_A)^{-1} \hat{B}^T \psi_A \end{pmatrix}, \quad \hat{M}\psi' = \hat{\varepsilon}^2\lambda\psi' + O(\hat{\varepsilon}^2) = O(\varepsilon^2) \quad (20)$$

meaning to first order in  $\hat{\varepsilon}$  the corrections to eigenvalues of slow modes vanishes. This is desired because the slow mode eigenvalues are  $O(\hat{\varepsilon}^2)$ . We also observe that slow modes of  $L$  are mostly confined to  $\mathbf{Slow}_\varepsilon[\hat{L}]$  and only get  $O(\varepsilon)$  contributions from the fast subspace of  $\hat{L}$ .

As a side, it follows that all weighted graphs share the null space of the unweighted Laplacian.

**Proposition C.3** (Shared null space). *Let  $\mathbf{Null}[M] = \text{Span}\{v | v \in \mathbb{R}^n, Mv = 0\}$  denote the null space of a matrix  $M \in \mathbb{R}^{n \times n}$ . The null space of the Laplacian  $\hat{L}$  (unweighted) is contained in the null space of Laplacian  $L$  (weighted), meaning  $\mathbf{Null}[\hat{L}] \subseteq \mathbf{Null}[L]$ .*

**Lemma C.4.**  $\text{Null}[\hat{L}] = \text{Null}[R^T]$

*Proof.*  $\forall v \in \text{Null}[\hat{L}], 0 = v^T \hat{L} v = \|\mathbb{R}^T v\|^2$  and  $\forall v \in \text{Null}[R^T], \hat{L} v = R R^T v = 0$ .  $\square$

*Proof of proposition C.3.*  $\forall v \in \text{Null}[\hat{L}], L v = R Q R^T v = 0$  hence,  $\text{Null}[\hat{L}] \subseteq \text{Null}[L]$ .  $\square$

Note that  $\text{Null}[\hat{L}]$  and  $\subseteq \text{Null}[L]$  are not necessarily the same because weights can be zero, which could make the null space of the weighted graph larger than the unweighted one. Next, we present our method for coarse-graining using a set of canonical slow modes.

## D Invariant additive dyadic potentials

We want to Compute the Hessian of equation 10,  $\mathcal{L}(X) = \sum_{ij} (r_{ij})$ . Let  $\hat{r} = \eta \mathbf{r} / r$  be the dual unit vector of  $\mathbf{r}$ . First, note that

$$\begin{aligned} \partial_i r_{jk} &\equiv \frac{\partial r_{jk}}{\partial X_i} = \partial_i \sqrt{\|X_j - X_k\|_\eta} \\ &= \eta \frac{r_{jk}}{r_{jk}} (\delta_{ij} - \delta_{ik}) = \hat{r}_{jk} (\delta_{ij} - \delta_{ik}) \end{aligned} \quad (21)$$

Then the gradient becomes

$$\begin{aligned} \partial_i \mathcal{L}(X) &= \sum_{j,k} f'_{jk}(r_{jk}) \frac{\partial r_{jk}}{\partial x_i} \\ &= \sum_{j,k} f'_{jk}(r_{jk}) \eta \hat{r}_{jk} (\delta_{ij} - \delta_{ik}) \\ &= 2 \sum_j f'_{ij}(r_{ij}) \eta \hat{r}_{ij}. \end{aligned} \quad (22)$$

where we used  $\hat{r}_{jk} = -\hat{r}_{kj}$  to show both terms in  $(\delta_{ij} - \delta_{ik})$  yield the same output. Finally, the Hessian becomes

$$\begin{aligned} [H(X)]_{ij} &= \partial_i \partial_j \mathcal{L}(X) = 2 \partial_j \sum_k f'_{ik}(r_{ik}) \hat{r}_{ik} \\ &= 2 \sum_k [f''_{ik}(r_{ik}) \partial_j r_{ik} \otimes \hat{r}_{ik} + f'_{ik}(r_{ik}) \partial_j \hat{r}_{ik}] \\ &= 2 \sum_k \left[ (\delta_{ji} - \delta_{jk}) f''_{ik}(r_{ik}) \hat{r}_{ik} \otimes \hat{r}_{ik} \right. \\ &\quad \left. + f'_{ik}(r_{ik}) \left( \eta \frac{\delta_{ji} - \delta_{jk}}{r_{ik}} - \frac{\hat{r}_{ik}}{r_{ik}^2} \partial_j r_{ik} \right) \right] \\ &= 2 \sum_k (\delta_{ji} - \delta_{jk}) \left[ f''_{ik}(r_{ik}) \hat{r}_{ik} \otimes \hat{r}_{ik} + f'_{ik}(r_{ik}) \left( \frac{\eta}{r_{ik}} - \frac{\hat{r}_{ik}}{r_{ik}^2} \otimes \hat{r}_{ik} \right) \right] \\ &= 2 \sum_k \left[ f''_{ik}(v) \hat{v} \otimes \hat{v} + \frac{f'_{ik}(v)}{v} (\eta - \hat{v} \otimes \hat{v}) \right]_{v=r_{ik}} (\delta_{ij} - \delta_{jk}) \\ &= 2 \sum_k \left[ \left( f''_{ik}(v) - \frac{f'_{ik}(v)}{v} \right) \hat{v} \otimes \hat{v} + \frac{f'_{ik}(v)}{v} \eta \right]_{v=r_{ik}} (\delta_{ij} - \delta_{jk}) \\ &= \sum_k \mathbf{H}_{ik}(x) (\delta_{ij} - \delta_{jk}) = \text{Lap}(\mathbf{H})_{ij} \end{aligned} \quad (23)$$

This is because the components of Laplacian can be be written

$$\begin{aligned} L_{ij} &= \text{Lap}(A)_{ij} = (D - A)_{ij} \\ &= \delta_{ij} \sum_k A_{ik} - A_{ij} = \sum_k A_{ik} (\delta_{ij} - \delta_{jk}) \end{aligned} \quad (24)$$

## D.1 Incidence matrix

The Laplacian  $L = D - A$  of an undirected graph with adjacency  $A$  can be written as  $L = CWC^T/2$  using the incidence matrix  $C$  and the edge weights  $W$ . This can be shown as follows

$$\begin{aligned}
[CWC^T]_{ij} &= \sum_e C_i^e W_{ee} C_j^e \\
&= \sum_{k,l} C_i^{(k \rightarrow l)} A_{kl} C_j^{(k \rightarrow l)} \\
&= \sum_{k,l} (\delta_{il} - \delta_{ik}) A_{kl} (\delta_{jl} - \delta_{jk}) \\
&= \sum_{k,l} (\delta_{il}\delta_{jl} - \delta_{ik}\delta_{jl} - \delta_{il}\delta_{jk} + \delta_{ik}\delta_{jk}) A_{kl} \\
&= 2 \sum_{k,l} (\delta_{il}\delta_{jl} - \delta_{ik}\delta_{jl}) A_{kl} \\
&= 2 \sum_k \delta_{ij} A_{kj} - 2A_{ij} = 2(D - A)_{ij} = 2L_{ij} \tag{25}
\end{aligned}$$

where we assumed  $A_{kl} = A_{lk}$  (undirected graph).

So the same derivation of the backbone also holds for this case. The idea is that using the incidence matrix  $C$  and edge weights  $W$  (as a diagonal matrix), any Laplacian  $L$  can be decomposed as  $L = CWC^T$ . Then, doing SVD  $C = USV^T$  we have

$$L = USV^T W V S^T U^T = U M U^T \tag{26}$$

Where the matrix  $M = SV^T W V S^T$  has an interesting property, namely that its null space includes the null space of the unweighted Laplacian  $L_0 = CC^T$ . To see this note that  $L_0 = US S^T S^T$ , which means columns  $U_i$  are the eigenvectors of  $L_0$  with eigenvalues  $S_i^2$ . The null eigenspace of  $L_0$  are the  $U_i$  for which  $S_i = 0$ . This subspace will also be a null subspace for  $L$ , because that block is also zero in  $M$ , because  $M_{ij} = \sum_c S_i V_{ik} W_{kk} V_{jk} S_j$ . So, whenever  $S_i = 0$  or  $S_j = 0$ ,  $M_{ij} = 0$ , meaning that whole block in  $M$  is zero and  $M U_i = 0$  (write it better).

**Example: power law.** Let  $f(r) = r^p$ . We have  $f' = pr^{p-1}$  and  $f'' = p(p-1)r^{p-2}$ , yielding the Hessian

$$\mathbf{H} = \nabla \nabla f(r) = r^{p-2} [(p^2 - 2p) \hat{r} \otimes \hat{r} + p\eta] \tag{27}$$

$$B_{ik} = A_{ik} r_{ik}^{p-2} [(p^2 - 2p) \hat{r}_{ik} \otimes \hat{r}_{ik} + p\eta] \tag{28}$$

**Example: Lennard-Jones.** This potential has the form

$$f(r) = 4\epsilon \left[ \left( \frac{\sigma}{r} \right)^p - \left( \frac{\sigma}{r} \right)^q \right] \tag{29}$$

where for classic van-der Waals potential  $p = 2q = 12$ . The Hessian for this potential is given by

$$\mathbf{H}(r) = \nabla \nabla f(r) = \epsilon \left[ \left( \frac{\sigma}{r} \right)^{p+2} [(p^2 + 2p) \hat{r} \otimes \hat{r} - p\eta] - \left( \frac{\sigma}{r} \right)^{q+2} [(q^2 + 2q) \hat{r} \otimes \hat{r} - q\eta] \right] \tag{30}$$

and  $B_{ik} = A_{ik} \mathbf{H}(r_{ik})$

## D.2 Structure and spectrum of $Q = V^T W V$

To consider only the relevant subspace of SVD, we have  $U, S \in \mathbb{R}^{n \times n}$ , and  $V \in \mathbb{R}^{m \times n}$ , with  $n = |\mathcal{V}|$  and  $m = |\mathcal{E}|$ . For a connected undirected graph  $m \geq 2(n-1)$  and  $V$  is full rank ( $V^T V = I_n$ ). Note the edge weights  $W$  come from the forces  $f_{ij}(r_{ij})$  in equation 13, which for an arbitrary  $X$  will be random. Assuming a Gaussian distribution  $W_{ee} \sim \mathcal{N}(0, \sigma)$  for all edges  $e$ , the matrix  $Q$

will also have random Gaussian entries. When  $m = n$ ,  $V$  defines the eigenbasis of  $Q$  and  $W_{ee}$  are the eigenvalues of  $Q$ . Similarly, in sparse graphs, where  $m \sim O(n)$ ,  $V$  is approximately the eigenbasis and the spectrum of  $Q$  should have a distribution similar to  $W_{ee}$ . For dense graphs, where  $m \sim O(n^2)$ , every entry of  $Q$  will involve a weighted sum over multiple  $W_{ee}$ . Then, from central limit theorem, entries of  $Q$  will asymptotically have a Gaussian distribution. From random matrix theory, we know that such  $Q$  will have a spectrum which follows the Wigner-semi-circle law. In both cases (sparse and dense graphs) the spectrum of  $Q$  has a finite variance and sits somewhere between a Gaussian and a semi-circle.

### D.3 Generalization to nonzero but small SV

We want to know how much the slow modes of weighted and unweighted graphs to overlaps. With the spectral expansion  $\hat{L} = \sum_i \lambda_i \psi_i \psi_i^T$  Define the slow subspace as in equation 15

$$\mathbf{Slow}_\varepsilon[\hat{L}] = \text{Span}\{\psi_i \mid |\lambda_i| < \varepsilon^2 \lambda_{\max}(\hat{L})\} \quad (31)$$

where  $\lambda_{\max}(\hat{L}) = \max\{\lambda_i\} = \max_\psi[\psi^T L \psi / \|\psi\|^2]$  is the largest eigenvalue of  $L$  and  $\varepsilon \ll 1$ . In terms of the singular values (SV) of the incidence matrix  $C = USV^T$ , the slow subspace becomes

$$\mathbf{Slow}_\varepsilon[\hat{L}] = \{i \mid S_{ii} < \varepsilon \max[S]\} \quad (32)$$

We will show that the slow modes in weighted  $L = CW C^T$  are perturbations to the slow modes of  $\hat{L}$ . Define

$$M = SV^T W V S^T = SQS^T \quad (33)$$

Normalize  $\hat{S} = S / \max[S]$ . Break the space down to the slow and fast subspaces, based on whether  $\hat{S}_{ii} < \varepsilon$  or not. First, since  $L$  is positive semi-definite, we can make all  $S_{ii} \geq 0$ . Let  $\hat{S} = S / \max S$ . We sort the dimensions in  $\hat{S}$  to have the small SVs appear first. Denote the block in  $\hat{S}$  where  $S_{ii} < \varepsilon$  by  $S_\varepsilon$ . We have

$$\hat{S}^2 = \begin{pmatrix} S_\varepsilon^2 & 0 \\ 0 & S_1^2 \end{pmatrix} < \begin{pmatrix} \varepsilon^2 & 0 \\ 0 & 1 \end{pmatrix} \quad (34)$$

We know the null space of  $\hat{L}$ , where  $S_{ii} = 0$ , is shared with  $L$ . First, we remove the null space from  $L$  and  $\hat{L}$ , calling the remainder  $L_0$  and  $\hat{L}_0$  and the remaining SVs  $\hat{S}$ . Then in this remainder subspace we need to find parts which are  $O(\varepsilon)$ . We sort the dimensions in  $\hat{S}$  to have the small SVs appear first. We denote the block in  $\hat{S}$  where  $S_{ii}^2 < \varepsilon \max[S^2]$  by  $S_\varepsilon$ . We have

$$M = \max[S]^2 \hat{S} Q \hat{S}^T = \begin{pmatrix} S_\varepsilon Q_{\varepsilon\varepsilon} S_\varepsilon & S_\varepsilon Q_{\varepsilon 1} S_1 \\ S_1 Q_{\varepsilon 1}^T S_\varepsilon & S_1 Q_{11} S_1 \end{pmatrix} = \begin{pmatrix} M_{\varepsilon\varepsilon} & M_{\varepsilon 1} \\ M_{\varepsilon 1}^T & M_{11} \end{pmatrix} \quad (35)$$

Because  $S_\varepsilon$  is  $O(\varepsilon)$  and  $S_1$  is  $O(1)$ , we will factor out the factors of  $\varepsilon$  from blocks in  $M$  and write

$$M = \max[S]^2 \begin{pmatrix} \varepsilon^2 A & \varepsilon B \\ \varepsilon B^T & C \end{pmatrix} \quad (36)$$

Here  $A$  and  $C$  are random matrices built from their corresponding blocks in  $Q$  and sandwiched between  $S_\varepsilon/\varepsilon$  (for  $A$ ), and  $S_1$  (for  $C$ ), which have  $O(1)$  values. The spectrum of  $Q$  has a distribution between a Gaussian with mean zero and a Wigner semi-circle, also centered around zero. We expect spectra of  $A$  and  $C$  to be similar to  $Q$ . Denote the spectral expansion of  $Q$  as

$$Q = \Psi \Lambda \Psi^T, \quad \Lambda = \text{diag}(\lambda_i)_{i=1}^n, \quad \Psi = [\psi_i]_{i=1}^n. \quad (37)$$

This is because when  $Q_{ij} \sim \mathcal{N}(0, \sigma)$  we have (ignoring Bessel's correction for  $k \gg 1$ ).

$$\sigma^2 = \text{Var}(Q_{ij}) \approx \frac{1}{n} \|Q\|^2 = \frac{1}{n} \sum_i \lambda_i^2 = \text{Var}(\Lambda) \quad (38)$$

where we assumed  $\text{Tr}[Q]/n \approx \text{mean}(Q) = 0$ . Since a block  $Q_k$  of size  $k$  is  $k^2$  entries sampled from the same distribution as  $Q$ , we expect

$$\frac{\|Q_k\|^2}{k^2} \approx \frac{\|Q_l\|^2}{l^2} \Rightarrow \frac{1}{k} \text{Var}(Q_k) \approx \frac{1}{l} \text{Var}(Q_l) \quad (39)$$

Thus, rescaling  $A \in \mathbb{R}^{n_A \times n_A}$  and  $C \in \mathbb{R}^{n_C \times n_C}$  we get

$$\hat{A} = \frac{A}{\sqrt{n_A}}, \quad \hat{C} = \frac{C}{\sqrt{n_C}}, \quad \text{Var}(\hat{A}) \approx \text{Var}(\hat{C}) \quad (40)$$

#### D.4 Approximate slow modes of $L$

If  $M$  did not have the off-diagonal blocks  $B$ , then  $\mathbf{Slow}_\varepsilon[L]$  and  $\mathbf{Slow}_\varepsilon[\hat{L}]$  would coincide, as the  $S_\varepsilon$  block and the  $S_1$  block would not mix when  $B = 0$ . Define  $M_0$  as the block matrix of  $M$  with  $B = 0$ .

$$M_0 \equiv \begin{pmatrix} \varepsilon^2 A & 0 \\ 0 & C \end{pmatrix} \quad (41)$$

Using spectral expansions

$$A = \Psi_A \Lambda_A \Psi_A^T, \quad C = \Psi_C \Lambda_C \Psi_C^T \quad (42)$$

the eigenvectors of  $M_0$  consist of

$$M_0 \begin{pmatrix} \psi_{Ai} \\ 0 \end{pmatrix} = \varepsilon^2 \lambda_{Ai} \begin{pmatrix} \psi_{Ai} \\ 0 \end{pmatrix}, \quad M_0 \begin{pmatrix} 0 \\ \psi_{Ci} \end{pmatrix} = \lambda_{Ci} \begin{pmatrix} 0 \\ \psi_{Ci} \end{pmatrix}. \quad (43)$$

Since we are looking for slow modes, we must also consider the magnitudes of  $\lambda_{Ai}$  and  $\lambda_{Ci}$ . Since  $A$  and  $C$  entries are random samples from  $Q$ , we expect them to have a semi-circle or Gaussian distribution similar to  $Q$ . Thus, we can use the variances of eigenvalues of  $A$  and  $C$  as a proxy for the how the magnitudes of  $\lambda_{Ai}$  and  $\lambda_{Ci}$  compare. From equation 40 we have

$$\frac{1}{n_A} \mathbb{E}[\Lambda_A^2] \approx \frac{1}{n_A} \text{Var}(A) \approx \frac{1}{n_C} \mathbb{E}[\Lambda_C^2] \quad (44)$$

Based on this we define a rescaled  $\hat{\varepsilon}$  such that  $\varepsilon^2 \lambda_{Ai}$  still has a smaller magnitude than  $\lambda_{Ci}$  on average, meaning we want

$$\varepsilon^4 \mathbb{E}[\Lambda_A^2] < \mathbb{E}[\Lambda_C^2] \quad \Rightarrow \quad \varepsilon^4 n_A < n_C \quad \Rightarrow \quad \hat{\varepsilon}^2 \equiv \varepsilon^2 \sqrt{\frac{n_A}{n_C}} < 1 \quad (45)$$

We choose  $\varepsilon$  such that the condition in equation 45 is satisfied. We can express  $M$  in terms of  $\hat{\varepsilon}$  by rescaling  $A$  and  $B$  to  $\hat{\varepsilon}^2 \hat{A} = \varepsilon^2 A$  and  $\hat{\varepsilon} \hat{B} = \varepsilon B$ . Now eigenvalues of  $\hat{A}$  have the same variance as eigenvalues of  $C$ . For brevity, denote  $\hat{M} = \max[S]^2 M$ . We have

$$\hat{M} = \begin{pmatrix} \hat{\varepsilon}^2 \hat{A} & \hat{\varepsilon} \hat{B} \\ \hat{\varepsilon} \hat{B}^T & C \end{pmatrix}. \quad (46)$$

To find how slow modes of  $\hat{M} = SQS^T / \max[S]^2$  differ from slow modes of  $SS^T$ , we break  $\hat{M}$  into a block diagonal part and an  $O(\hat{\varepsilon})$  off-diagonal perturbation

$$\hat{M} = M_0 + \hat{\varepsilon} \delta M, \quad M_0 = \begin{pmatrix} \hat{\varepsilon}^2 \hat{A} & 0 \\ 0 & C \end{pmatrix} \quad \delta M = \begin{pmatrix} 0 & \hat{B} \\ \hat{B}^T & 0 \end{pmatrix}. \quad (47)$$

As in equation 43, eigenvectors of  $A = \sqrt{n_C/n_A} \hat{A}$  and  $C$  are eigenvectors of  $M_0$ . Now we want to find eigenvectors of  $\hat{M}$  with small  $O(\varepsilon^2)$  eigenvalues up to order  $\hat{\varepsilon}$  corrections by treating  $\delta M$  as a perturbation.

$$\begin{aligned} (M_0 + \hat{\varepsilon} \delta M)(\psi + \hat{\varepsilon} \delta \psi) &= (\lambda + \hat{\varepsilon} \delta \lambda)(\psi + \hat{\varepsilon} \delta \psi) \\ M_0 \psi + \hat{\varepsilon} (\delta M \psi + M_0 \delta \psi) + O(\hat{\varepsilon}^2) &= \lambda \psi + \hat{\varepsilon} (\delta \lambda \psi + \lambda \delta \psi) + O(\hat{\varepsilon}^2) \\ \Rightarrow \delta M \psi + M_0 \delta \psi &= \delta \lambda \psi + \lambda \delta \psi \end{aligned} \quad (48)$$

We only need the components of  $\delta \psi$  orthogonal to  $\psi$ , so we can assume  $\delta \psi^T \psi = 0$ . From this we have

$$\delta \lambda = \psi^T \delta M \psi + \psi^T M_0 \delta \psi = \psi^T \delta M \psi, \quad (49)$$

where we used  $\psi^T M_0 \delta \psi = \lambda \psi^T \delta \psi = 0$ . Plugging equation 49 into equation 48 we can solve for  $\delta \psi$  by inverting the matrices

$$\begin{aligned} (M_0 - \lambda) \delta \psi &= (\delta \lambda - \delta M) \psi \\ \Rightarrow \delta \psi &= (M_0 - \lambda + i\eta)^{-1} (\delta \lambda - \delta M) \psi \end{aligned} \quad (50)$$

where we added a small  $\eta$  to make the matrix  $M_0 - \lambda$  invertible, as  $\lambda$  is one of its eigenvalues.

To find slow modes, we start from slow modes of  $M_0$  which are in the  $A$  subspace. Let  $\psi_A$  be an eigenvector of  $A$  with  $\hat{A}\psi_A = \lambda_A\psi_A$ . Concatenating  $\psi_A$  with zeros in the  $C$  subspace we have

$$\psi = \begin{pmatrix} \psi_A \\ 0 \end{pmatrix}, \quad M_0\psi = \hat{\varepsilon}^2\lambda_A\psi. \quad (51)$$

Using this  $\psi$  to compute  $\delta\lambda$  in equation 49 we have

$$\delta\lambda = \psi^T \delta M \psi = (\psi_A^T \ 0) \begin{pmatrix} 0 \\ \hat{B}^T \psi_A \end{pmatrix} = 0 \quad (52)$$

meaning to first order in  $\hat{\varepsilon}$  the corrections to eigenvalues of slow modes vanishes. This is desired because the slow mode eigenvalues are  $O(\hat{\varepsilon}^2)$  and we find that with this  $\psi$  ansatz the corrections it will get are also at least  $O(\hat{\varepsilon}^2)$ . Next, we compute the corrections  $\delta\psi$  to the eigenvectors. Plugging  $\psi$  into equation 50 with  $\lambda = \hat{\varepsilon}^2\lambda_A$  and  $\delta\lambda = 0$  we have

$$\begin{aligned} (M_0 - \lambda + i\eta)^{-1} &= \begin{pmatrix} (\hat{\varepsilon}^2\hat{A} - \lambda + i\eta)^{-1} & 0 \\ 0 & (C - \lambda)^{-1} \end{pmatrix} \\ \delta\psi &= -(M_0 - \lambda + i\eta)^{-1} \delta M \psi \\ &= \begin{pmatrix} 0 \\ (C - \lambda)^{-1} \hat{B}^T \psi_A \end{pmatrix} \end{aligned} \quad (53)$$

where we dropped  $i\eta$  in the lower block because  $\hat{\varepsilon}^2\lambda_A$  is unlikely to be also an eigenvalue of  $C$ , as  $A$  and  $C$  are random matrices.

Using the relation  $\hat{\varepsilon}\hat{B} = \varepsilon B$  with the original  $\varepsilon$  and putting all together we find the eigenvector  $\psi' = \psi + \hat{\varepsilon}\delta\psi$  up to order  $O(\hat{\varepsilon}^2)$  to be

$$\psi' = \begin{pmatrix} \psi_A \\ \hat{\varepsilon}(C - \hat{\varepsilon}^2\lambda_A)^{-1} \hat{B}^T \end{pmatrix} \quad (54)$$

$$\hat{M}\psi' = \hat{\varepsilon}^2\lambda\psi' + O(\hat{\varepsilon}^2) = O(\hat{\varepsilon}^2) \quad (55)$$